Rock Mech Rock Eng (2018) 51:811–825
https://doi.org/10.1007/s00603-017-1348-2

ORIGINAL PAPER

A Novel DEM Approach to Simulate Block Propagation on Forested Slopes

David Toe[1,2] · Franck Bourrier[1,2] · Luuk Dorren[3] · Frédéric Berger[1,2]

Received: 25 January 2017 / Accepted: 15 October 2017 / Published online: 27 October 2017

Abstract In order to model rockfall on forested slopes, we developed a trajectory rockfall model based on the discrete element method (DEM). This model is able to take the complex mechanical processes at work during an impact into account (large deformations, complex contact conditions) and can explicitly simulate block/soil, block/tree contacts as well as contacts between neighbouring trees. In this paper, we describe the DEM model developed and we use it to assess the protective effect of different types of forest. In addition, we compared it with a more classical rockfall simulation model. The results highlight that forests can significantly reduce rockfall hazard and that the spatial structure of coppice forests has to be taken into account in rockfall simulations in order to avoid overestimating the protective role of these forest structures against rockfall hazard. In addition, the protective role of the forests is mainly influenced by the basal area. Finally, the advantages and limitations of the DEM model were compared with classical rockfall modelling approaches.

Keywords Rockfall · Impact · DEM · Slope · Tree

List of symbols

α	Viscous damping coefficient
α_{cr}	Critical damping coefficient
α_s	Local slope between two spheres constituting the soil
$\frac{dU_n^{soil}}{dt}$	Relative velocity between the spheres in the direction normal to the contact surface
κ_{soil}	Ratio between K_t^{soil} and K_n^{soil}
ν	Poisson ratio of a stem
σ_{Elast}	Elastic bending stress limit
σ_{Rupt}	Rupture bending stress
τ	Damping coefficient
$d\dot{\theta}_x$	Increment of the relative rotational velocity between two nodes around x axis
$d\dot{\theta}_y$	Increment of the relative rotational velocity between two nodes around y axis
$d\Delta\sigma_{1\_2,x}$	Increment of relative orientation of the local coordinate systems of node 1 and node 2 around x axis
$d\Delta\sigma_{1\_2,y}$	Increment of relative orientation of the local coordinate systems of node 1 and node 2 around y axis
dF_t^{soil}	Increment of tangential force
dM_x^{Damp}	Contributions of the damping to the interaction moments around x axis
dM_y^{Damp}	Contributions of the damping to the interaction moments around y axis
dM_x^{Root}	Increment of moment added to the moment M_x^{Root}
dM_y^{Root}	Increment of moment added to the moments M_y^{Root}
dU_t^{soil}	Relative increment of tangential displacement between the block and the soil at the contact point
θ_x	Relative orientation of the local coordinate systems associated with the adjacent nodes around x axis

✉ David Toe
david.toe@irstea.fr

[1] IRSTEA, 2, Rue de la Papeterie, 38402 Saint-Martin-d'Hères, France

[2] Université Grenoble Alpes, 38402 Grenoble, France

[3] Department of Forest Science, Bern University of Applied Sciences, Langgasse 85, 3052 Zollikofen, Switzerland

θ_y	Relative orientation of the local coordinate systems associated with the adjacent nodes around y axis
φ^{soil}	Friction angle associated with the interaction between the block and the soil
$\varphi^{\text{b\_t}}$	Friction angle associated with the interaction between a block and a tree
$\varphi^{\text{t\_t}}$	Friction angle associated with the interaction between two trees
ξ	Heaviside function
A	Forests integrating the spatial aggregation of the stems
d	Distance between two spheres constituting the soil
D_{Con}	Mean tree diameter between the nodes
d_{obs}	Mean nearest neighbour distance in the pattern
D_{Stem}	Tree diameter at breast height
D_1	Block first principal axis
D_2	Block second principal axis
D_3	Block third principal axis
$\text{Dist}^{50}_{\text{NF}_{\text{DEM}}}$	Distances where 50% of the blocks were stopped in the simulations without forest from the DEM model
$\text{Dist}^{50}_{\text{NF}_{\text{RF3D}}}$	Distances where 50% of the blocks were stopped in the simulations without forest from RF3D
$\text{Dist}^{50}_{\text{WF}_{\text{DEM}}}$	Distances where 50% of the blocks were stopped in the simulations with forest from the DEM model
$\text{Dist}^{50}_{\text{WF}_{\text{RF3D}}}$	Distances where 50% of the blocks were stopped in the simulations with forest from RF3D
E_{Plast}	Equivalent modulus for the first linear relation
E_{Unld}	Equivalent modulus for the unloading linear relation
E_{b}	Young modulus of the block
e_{n}	Normal restitution coefficient defined at the contact point between the block and the soil
E_{r}	Radial elasticity modulus of fresh wood
E_{d}	Mean nearest neighbour distance expected for a Poisson point process of the same intensity
F^{soil}	Contact force between a block and the soil
$F^{\text{b\_t}}$	Contact force between the block and a tree
$F^{\text{t\_t}}$	Contact force between two trees
$F^{\text{soil}}_{\text{n}}$	Normal component of the contact force between a block and the soil
$F^{\text{b\_t}}_{\text{n}}$	Normal component of the contact force between a block and a tree
$F^{\text{t\_t}}_{\text{n}}$	Normal component of the contact force between two trees
$F^{\text{soil}}_{\text{t}}$	Tangential component of the contact force between a block and the soil
$F^{\text{b\_t}}_{\text{t}}$	Tangential component of the contact force between a block and a tree
$F^{\text{t\_t}}_{\text{t}}$	Tangential component of the contact force between two trees
G	Basal area
$g(r)$	Pair density function
H_{T}	Length of the tree, including the crown
I	Bending moment of inertia associated with the z-axis
K_{Elast}	Stiffness coefficient associated with the first linear relation
K_{Plast}	Stiffness coefficient associated with the second linear relation
K_{Root}	Stiffness coefficient associated with the behaviour of the root system
K_{Unld}	Stiffness coefficient associated with the unloading linear relation
$K^{\text{soil}}_{\text{n}}$	Normal stiffness coefficient associated with the interaction between the block and the soil trees
$K^{\text{b\_t}}_{\text{n}}$	Normal stiffness coefficient associated with the interaction between between the block and a tree
$K^{\text{t\_t}}_{\text{n}}$	Normal stiffness coefficient associated with the interaction between two trees
$K^{\text{t\_t}}_{\text{t}}$	Tangential stiffness coefficient associated with the interaction between two trees
$K^{\text{soil}}_{\text{t}}$	Tangential stiffness coefficient associated with the interaction between the block and the soil trees
$K^{\text{b\_t}}_{\text{t}}$	Tangential stiffness coefficient associated with the interaction between between the block and a tree
l	Distance between two nodes
L_{C}	Length of the crown
M_{a}	Threshold moment associated with the root rupture
M_{Elast}	Threshold moment associated with the occurrence of plastic strain
M_{Root}	Bending moment applied to the root system
M_{Rupt}	Threshold moment associated with the tree stem breakage
M^{Root}_x	Bending moment applied to the base of the tree stem around x axis
M^{Root}_y	Bending moment applied to the base of the tree stem around y axis
m_{C}	Mass of the crown
m_{b}	Mass of the block
m_{N}	Additional mass assigned to nodes belonging to the crown

M_x	Bending moment around x axis
M_y	Bending moment around y axis
Mean_D	Mean diameters of the trees in a forest
MOE	Modulus of elasticity
N	Number of stems per hectare
N_{E_d}	Number of trees in the forest
NA	Forests generated without spatial stem aggregation
$\text{PF}^{50}_{\text{DEM}}$	Protection index determined from the run-out distances of the DEM model
$\text{PF}^{50}_{\text{RF3D}}$	Protection index determined from the run-out distances of RF3D
r	Distance between two trees
R_{Clark}	Clark and Evans aggregation index
R_{soil}	Radius of spheres constituting the soil
R_b	Radius of a sphere constituting the block
r_b	Radius of the block
r_s	Radius of a connection
R_{s1}	Radius of the stem 1 at the interaction point
R_{s2}	Radius of the stem 2 at the interaction point
S	Surface of the forest
Std_D	Standard deviation of the diameters of the trees in a forest
U^{soil}_n	Normal overlap between the block and the soil
$U^{\text{b\_t}}_\text{n}$	Normal overlap between the block an a tree in the direction normal to the contact surface
$U^{\text{t\_t}}_\text{n}$	Normal overlap between two trees in the direction normal to the contact surface

1 Introduction

Rockfall is a natural hazard that endangers infrastructure and residential areas worldwide. On forested slopes, foresting and lying trees can, however, mitigate this rockfall hazard due to the energy dissipation during a tree impact (Volkwein et al. 2011). The efficiency of a forest mainly depends on the mass of the falling rock, its velocity, the tree diameter distribution in the forest, the basal area (sum of the cross-sectional area of all tree trunks 1.3 m above ground within 1 ha of the study area) and the length of the forested slope (Dupire et al. 2016; Toe et al. 2017). Only a few rockfall trajectory models explicitly take into account forests (spatial tree distribution, distribution of tree diameters and tree species) and their mitigating effect (Volkwein et al. 2011). These models mostly integrate the forest's protective effect based on empirical relationships which describe the block trajectory deviation and the energy loss as a function of the tree diameter, the impact height and the eccentricity of the block impact on the trunk (Dorren and Berger 2006; Jancke 2012). However, these relationships do not integrate all the physical processes occurring during block/tree or tree/tree impacts.

The calculation of the block's reflected trajectory after an impact on a tree requires a numerical model describing the mechanical response of the tree during the impact. In recent years, advanced methods to model the dynamic response of a tree subjected to the impact of a block have been proposed by several authors. Jonsson et al. (2007) and Bertrand et al. (2013) have proposed models based on the finite element method (FEM). The model proposed by Jonsson et al. (2007) includes, in particular, the contact between the block and the tree (spruce) and the role of the root system. Toe et al. (2017) proposed a model to simulate the impact of blocks on a tree based on the discrete element method (DEM). In this approach, the tree is represented as a deformable beam and the contact between the block and the tree is modelled explicitly. The use of this method provides a more simplified modelling of the tree compared to FEM modelling, with the advantage of being more efficient in terms of computation time.

Over the past few years, rockfall models using the DEM have proved their ability to model rockfall propagation integrating block shape, block fragmentation and protection structures (Plassiard and Donzé 2010; Xinpo et al. 2010; Thoeni et al. 2013, 2014). However, forest effects have not yet been integrated into DEM-based rockfall models.

This paper proposes a novel approach to integrate the protective role of forest against rockfall hazard in a DEM-based rockfall model. The proposed approach is used to simulate block trajectories through forest in order to quantify their protection function. Finally, the results obtained are compared with block trajectories simulated using a probabilistic lumped-mass model, called RockyFor3D (Dorren 2012) to identify the advantages and limitations of the model proposed.

2 Materials and Methods

2.1 DEM Rockfall Model

The model developed is based on a DEM approach (Cundall and Strack 1979) using the open-source code Yade-DEM (Šmilauer et al. 2014). One advantage of this method is that the interactions between a block, the soil and the trees are explicitly taken into account. The trees and the soil are modelled as assemblies of rigid, locally deformable spheres interacting by contact and/or remote forces. The resolution scheme of this method is based on an explicit time-stepping algorithm. At each time step, contact forces calculated from the particle locations and relative velocities are applied to all overlapping particles. The motion of the particles during the time step is then determined by solving Newton's equations, which allows updating the locations and velocities of

the particles for the following time step (Cundall and Strack 1979).

2.1.1 Modelling the Block and the Soil

The soil is modelled as an unbreakable assembly of spheres as in the block trajectory model CRSP-3D (Andrew et al. 2012). Successions of spheres are generated along a slope profile or along a surface corresponding to a digital terrain model (DTM). The diameter of each sphere of the soil is constant and set to 1.4 m following the same approach as in Andrew et al. (2012). The distance between adjoining spheres is set constant in order to generate a constant roughness along the profile (Fig. 6). This modelling approach integrates both the macroscopic topography, using a DTM or a slope profile, and the local topography changes, as a local roughness modelled by the spheres composing the slope surface.

In this study, we analyse the propagation of cubic blocks because it is a simple and realistic block shape. Each block is made of an unbreakable assembly of 27 spheres with identical diameters. The radius of each of these spheres (R_b) is calculated as follows:

$$R_b = \frac{D_1}{4} \tag{1}$$

R_b is the radius of a sphere constituting the block. D_1 is one of the block dimensions ($D_1 = D_2 = D_3$) (Fig. 1).

2.1.2 Modelling the Tree

Both single trees and coppice stools composing mountain forests (Jancke et al. 2009) are integrated into the model. Coppice stools are characterized as a tree stems belonging to the same stump. The tree stems are modelled as flexible cones according to the approach developed in Bourrier et al. (2013).

The cones are represented as chains of nodes linked by cylindrical connections that can be considered as chains of interconnected cylinders with radii decreasing from the bottom to the top of the tree. Interaction forces between the impacting block and the connections allow characterizing block/tree contacts, while interaction forces between the nodes allow modelling the stem as a deformable beam (Fig. 2). The stem mass is distributed along the stem and assigned to the corresponding nodes following the assumption that the stem is conical. The interaction forces and torques are applied to adjacent nodes along the stem's main axis (z) and along two axes perpendicular to the z-axis (x and y). The interaction forces along the z-axis are related to tensile loadings, while those along the other axes are associated with shear loadings. In addition, the interaction torques along the z-axis are related to twist loadings, while those along the y and x-axes are associated with bending loadings (Toe et al. 2017).

We assumed that no substantial tensile and twist loading develops because of the sliding of the block along the stem. In addition, the impact location is assumed far enough from the root system so that the shear stresses remain small compared to bending stresses. Consequently, the normal, shear, and twist induced forces and torques are modelled using linear elastic relationships between the node position (resp. orientations) and interaction forces (resp. moment) depending on the modulus of elasticity (MOE) and the Poisson ratio of the stem (ν) (Bourrier et al. 2013; Olmedo et al. 2016). The interaction torques

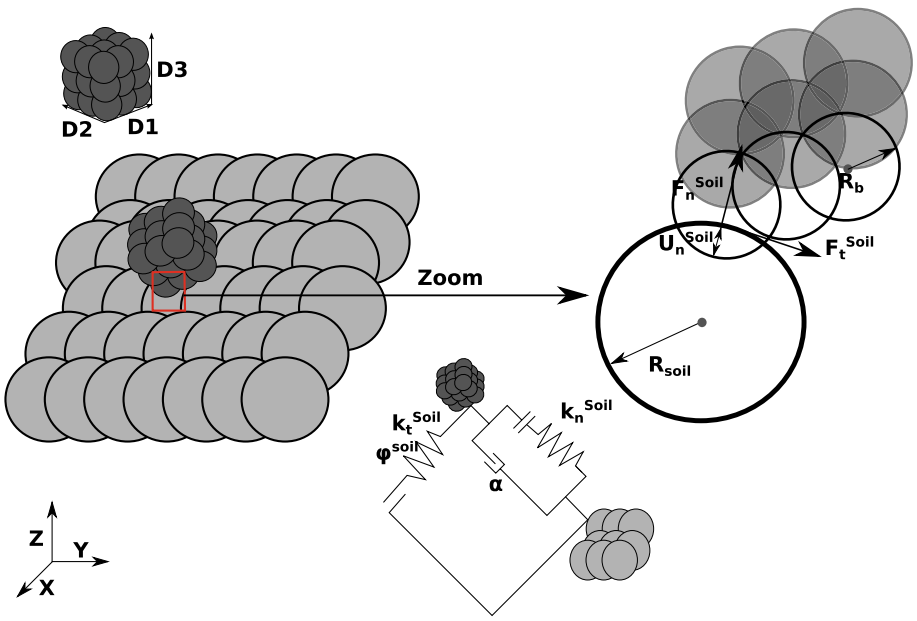

Fig. 1 Sketch of the interaction between the block and the soil. $D_1 = D_2 = D_3$ are the dimensions of the block. R_b and R_{soil} are, respectively, the radius of spheres constituting the block and the radius of spheres constituting the soil. U_n^{soil} is the overlap between the block and the soil. F_n^{soil} and F_t^{soil} F_t^{soil}Tangential stiffness at the contact surface are the normal force and the tangential force at the contact surface between the block and the soil. K_n^{soil} and K_t^{soil} are the normal stiffness and tangential stiffness at the contact surface. α is the viscous damping coefficient and φ^{soil} is the friction angle at the contact point

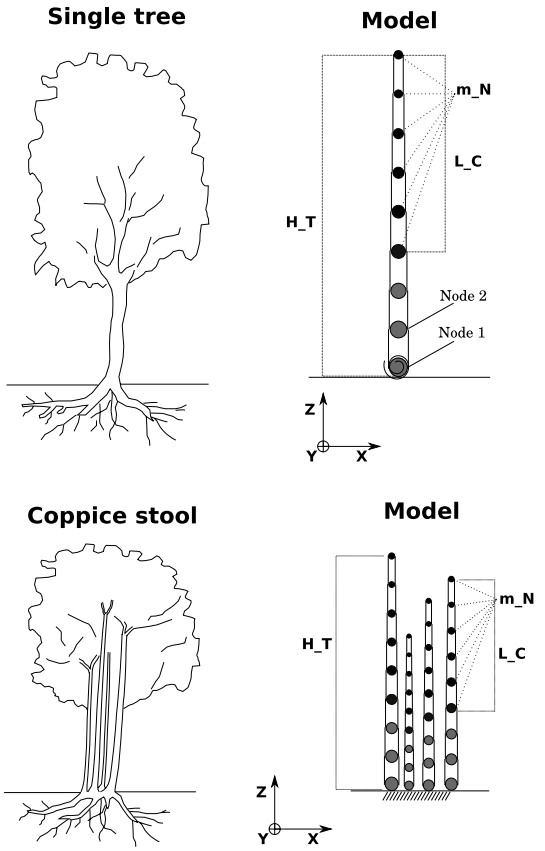

Fig. 2 Sketch of a single tree and a coppice stool and corresponding DEM models. L_C is the length of the crown. m_N is the additional mass assigned to nodes belonging to the crown. H_T is the length of the tree, including the crown. The root system is modelled by a rotation spring depending on the orientation of the local coordinate systems associated with node 1 and node 2

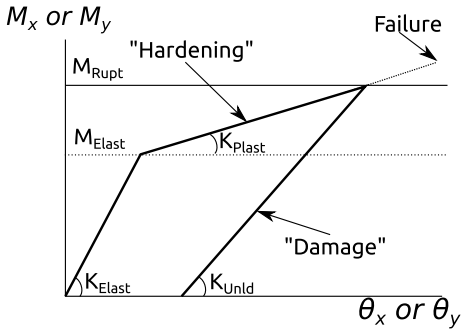

Fig. 3 Diagram representing the trilinear interaction law for the calculation of the bending moments between contiguous nodes (Olmedo et al. 2016)

between adjacent nodes in bending (i.e. along x and y axes) are calculated incrementally using a multi-linear relationship between the bending moments M_x and M_y and the relative orientation of the local coordinate systems associated with the adjacent nodes θ_x and θ_y (Fig. 3).

During the loading phase the relationship between M_x (resp. M_y) and θ_x (resp. θ_y) is described by a linear relationship characterized by a stiffness coefficient K_{Elast}. Once the threshold value M_{Elast} is reached, a second linear relationship characterized by a stiffness coefficient K_{Plast} is used. The unloading phase is also linear. It is associated with a stiffness coefficient K_{Unld}.

If the threshold M_{Rupt} is reached, the tree stem breaks, which leads to a complete loss of the mechanical resistance along all axes. The coefficients involved in the bending torque/orientation relationships are related to the geometrical and mechanical properties of the stem (Eqs. 2, 3, 4).

$$K_{\text{Elast}} = \frac{\text{MOE} \times I}{l} \tag{2}$$

$$K_{\text{Plast}} = \frac{E_{\text{Plast}} \times I}{l} \tag{3}$$

$$K_{\text{Unld}} = \frac{E_{\text{Unld}} \times I}{l} \tag{4}$$

MOE, E_{Plast} and E_{Unld} are the equivalent modulus for the first, second and unloading linear relations of the stem response. l is the distance between two nodes. I is the bending moment of inertia associated with the z-axis ($I = \frac{\pi \times D_{\text{Con}}^4}{64}$). D_{Con} is the mean tree diameter between the nodes considered.

The bending moment threshold (M_{Elast}), setting the limit between the first and the second linear relationships, is associated with the bending stress σ_{Elast} (Eq. 5).

$$M_{\text{Elast}} = \frac{\sigma_{\text{Elast}} \times I \times 2}{D_{\text{Con}}} \tag{5}$$

Similarly, the maximum bending moment (M_{Rupt}) is associated with the equivalent rupture stress (σ_{Rupt}) (Eq. 6).

$$M_{\text{Rupt}} = \frac{\sigma_{\text{Rupt}} \times I \times 2}{D_{\text{Con}}} \tag{6}$$

Although the relationships used in Eqs. (2), (3), (4), (5), and (6) are only valid for elastic material, we also used them when materials non-linearities developed for consistency purposes.

A viscous damping of the bending moments is integrated to adequately model the response of a fresh wood stem under dynamic loading (Olmedo 2015). The contributions of the damping $\mathrm{d}M_x^{\text{Damp}}$ and $\mathrm{d}M_y^{\text{Damp}}$ to the interaction moments are calculated as follows:

$$\mathrm{d}M_x^{\text{Damp}} = \tau \times K_{\text{Elast}} \times \mathrm{d}\dot{\theta}_x \tag{7}$$

$$\mathrm{d}M_y^{\text{Damp}} = \tau \times K_{\text{Elast}} \times \mathrm{d}\dot{\theta}_y \tag{8}$$

$d\dot{\theta}_x$ and $d\dot{\theta}_y$ are the increments of the relative rotational velocity between the nodes considered along the x and y axes. τ is the damping coefficient. This damping formulation is assumed to favour damping of high-vibration frequencies analogous to Rayleigh formalism according to Chopra (2011).

dM_x^{Damp} (resp. dM_y^{Damp}) is added to the interaction moment M_x (resp. M_y).

To take the influence of the root systems on single trees' behaviour during an impact into account, a bending moment was applied to the base of the tree stem depending on its orientation along the x and y axes (Toe et al. 2017) (Fig. 2) and following an elastic-perfectly plastic constitutive model. The bending moment was applied depending on the relative orientation of the local coordinate systems of node 1 and node 2 along the x and y axes using an incremental formalism.

$$dM_x^{\text{Root}} = K_{\text{Root}} \times d\Delta\sigma_{1\_2,x} \tag{9}$$

$$dM_y^{\text{Root}} = K_{\text{Root}} \times d\Delta\sigma_{1\_2,y} \tag{10}$$

where, K_{root} is a stiffness coefficient. dM_x^{Root} and dM_y^{Root} are the increment of moment added to the moments M_x^{Root} and M_y^{Root} along the x and y axes. $d\Delta\sigma_{1\_2,x}$ and $d\Delta\sigma_{1\_2,y}$ are the increment of relative orientation of the local coordinate systems of node 1 and node 2 along the x and y axes.

In addition, M_{Root} is limited to a threshold moment M_a (Dupuy et al. 2005; Lundström 2009).

Coppice stools are modelled as assemblies of stems that are fully embedded in the soil. This modelling assumption is based on the work of Jancke (2012), which highlights the small influence of the root system of the coppice stool on the block energy reduction. The position of the stems in a stool and their diameters are defined in agreement with field inventories (Sect. 2.2.2).

The length of the single trees and of the stems of a stool (H_T), including the length of the crown (L_C), are defined according to allometric relationships developed for beech (*Fagus sylvatica*) (Quetel 2005). The crown of the stems is modelled by an additional mass (m_C) uniformly distributed along a distance L_C from the top of the tree. The m_C was calculated using allometric relationships from Bartelink (1997)

$$H_T = 1.3 + (73.805 \times D_{\text{Stem}}) - (54.734 \times D_{\text{Stem}}^2) \tag{11}$$

$$L_C = 0.40642 \times H_T \tag{12}$$

$$m_C = 0.0031 \times D_{\text{Stem}}^{3.161} \tag{13}$$

D_{Stem} is the tree diameter at breast height.

2.1.3 Interactions

In the DEM model, the contacts between the block and the soil, the block and the stem and between the stems were modelled by forces applied at the contact points. These forces were calculated using the interpenetration and relative velocities between the objects. Each contact force (F) is split into a normal component to the contact surface (F_n) and a tangential component to that surface (F_t).

Block/Soil Interaction The interaction forces between the block and the soil are calculated using the interactions between the spheres which constitute the block and the soil (Fig. 1). The energy dissipated at the contact between the block and the soil is modelled by a viscous damping in the direction normal to the contact surface (Thoeni et al. 2014).

$$F_n^{\text{soil}} = K_n^{\text{soil}} \times U_n^{\text{soil}} + \alpha \frac{dU_n^{\text{soil}}}{dt} \tag{14}$$

F_n^{soil}, K_n^{soil} and U_n^{soil} are respectively the force, the stiffness and the overlap between two spheres in the direction normal to the contact surface. α is a viscous damping coefficient and $\frac{dU_n^{\text{soil}}}{dt}$ is the relative velocity between the spheres in the direction normal to the contact surface.

The damping coefficient α can be related to the normal restitution coefficient e_n defined at the contact point using Eq. (14).

$$\frac{\alpha}{\alpha_{cr}} = \frac{-\ln(e_n)}{\sqrt{\pi^2 + \ln^2(e_n)}} \tag{15}$$

α_{cr} is the critical damping coefficient defined as in Eq. (15)

$$\alpha_{cr} = 2 \times \sqrt{K_n^{\text{soil}} \times m_b} \tag{16}$$

m_b is the mass of the block.

The tangential force to the contact surface (F_t^{soil}) is directed in the opposite direction to the relative tangential velocity between two bodies in contact. This force is calculated incrementally from the relative displacement between the spheres at the contact point. At each time step, the increment of tangential force (dF_t^{soil}) is added to the tangential force calculated at the previous time step.

$$dF_t^{\text{soil}} = K_t^{\text{soil}} \times dU_t^{\text{soil}} \times \xi(F_n^{\text{soil}} \times \tan(\varphi^{\text{soil}}) - F_t^{\text{soil}})) \tag{17}$$

dU_t^{soil} is the relative increment of tangential displacement between the block and the soil at the contact point. K_t^{soil} is the tangential stiffness. φ^{soil} is the friction angle. ξ is the Heaviside function: $\xi(x) = 1$ if $x > 0$ and $\xi(x) = 0$ if $x \leq 0$.

The tangential force is limited in agreement with the Coulomb criterion:

$$| F_t | \leq F_n \times \tan(\varphi^{soil}) \tag{18}$$

The tangential stiffness is defined in relation to the normal stiffness using the κ_{soil} ratio:

$$\kappa_{soil} = \frac{K_t^{soil}}{K_n^{soil}} \tag{19}$$

Block/Stem and Stem/Stem Interactions The interaction forces between the block and a stem ($F_n^{b\_t}$ and $F_t^{b\_t}$) (Fig. 4) or between two stems ($F_n^{t\_t}$ and $F_t^{t\_t}$) (Fig. 5) are modelled by forces applied to the contact surface (Bourrier et al. 2013). These forces are calculated from the interpenetration and relative velocities between the objects in contact. In this study, the energy dissipated due to the permanent stem deformation at the contact surface was ignored compared to the energy dissipated due to the deformation of the stems during the impact. Thus, $F_n^{b\_t}$ and $F_n^{t\_t}$ were calculated using elastic relationships:

$$F_n^{b\_t} = K_n^{b\_t} \times U_n^{b\_t} \tag{20}$$

$K_n^{b\_t}$ is the normal stiffness. $U_n^{b\_t}$ is the overlap between the block and a connection.

$$F_n^{t\_t} = K_n^{t\_t} \times U_n^{t\_t} \tag{21}$$

$U_n^{t\_t}$ is the overlap between two connections.

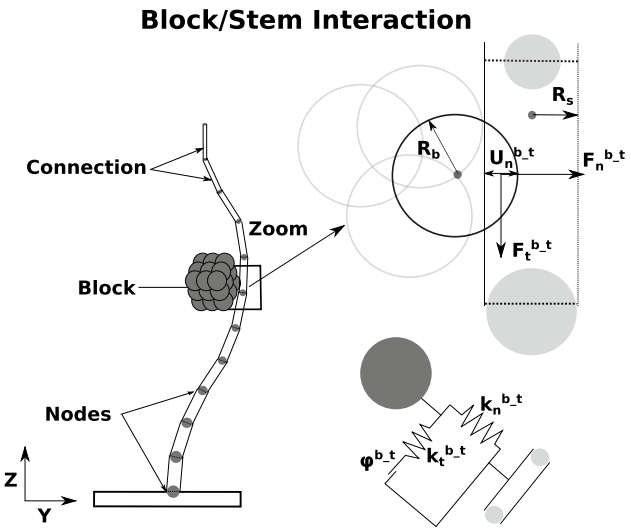

Fig. 4 DEM models of the tree impacted by a block. $U_n^{b\_t}$ is the block overlap with the tree, R_b and R_s are the block radius and tree radius at the contact surface. $F_n^{b\_t}$ and $F_t^{b\_t}$ are the normal and the tangential forces to the contact surface between the block and the tree. $K_n^{b\_t}$ is the normal stiffness, $K_t^{b\_t}$ is the tangential stiffness of the contact and φ^{b_t} is the friction angle

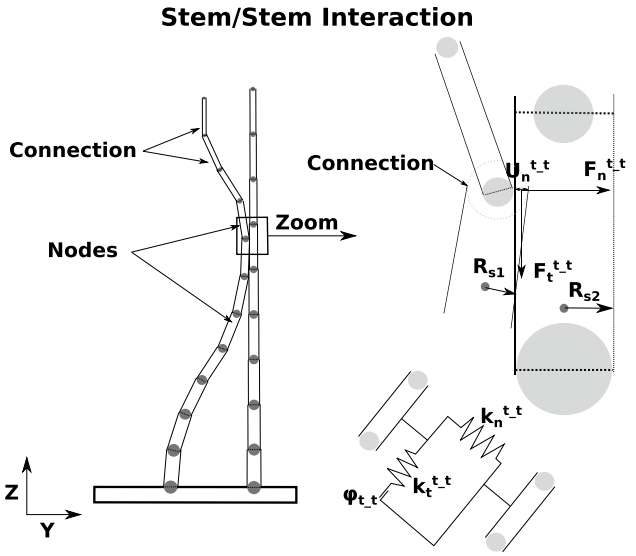

Fig. 5 DEM models of tree/tree interactions. $U_n^{t\_t}$ is the block overlap with the stem, R_{s1} and R_{s2} are the radius of the first and second tree at the contact surface. $F_n^{t\_t}$ and $F_t^{t\_t}$ are the normal and the tangential forces to the contact surface between the stems. $K_n^{t\_t}$ is the normal stiffness of the contact, $K_t^{t\_t}$ is the tangential stiffness of the contact and φ^{t_t} is the friction angle

The normal stiffness coefficients characterizing these linear relationships are related to the radial elasticity modulus of fresh wood (E_r) and the Young modulus of the block for block/stem interactions (E_b) (Eq. 21) and are only related to the radial elasticity modulus of fresh wood (E_r) for stem/stem interactions (Eq. 22).

$$K_n^{b\_t} = \frac{2 \times E_r \times r_s \times E_b \times r_b}{E_b \times r_b + E_r \times r_s} \tag{22}$$

r_b is the radius of the block and $r_s = \frac{D_{Con}}{2}$.

$$K_n^{t\_t} = \frac{2 \times E_r \times R_{s1} \times R_{s2}}{(R_{s1} + R_{s2})} \tag{23}$$

R_{s1} and R_{s2} are the radii of the stems at the interaction point.

The tangential force between two block/stem ($F_t^{b\_t}$) or stem/stem ($F_t^{t\_t}$) interactions are calculated in a similar manner as the tangential force between the block and the soil. The parameters for the calculation of the tangential force between the block and a stem are: the ratio between the normal stiffness and the tangential stiffness (κ_{b_t}) and the friction angle at the surface of contact (φ^{b_t}). The parameters for the calculation of the tangential force between two stems are: the ratio between the normal stiffness and the tangential stiffness (κ_{t_t}) and the friction angle at the surface of contact (φ^{t_t}).

2.2 Modelling the Block Propagation Along a Slope

2.2.1 Slope Studied

The topography used for this study was a virtual slope built following three steps.

The first step consisted of building a slope profile representative of the slopes located in the vicinity of the city of Grenoble. The slope profile was extracted from a DTM of the Vercors Mountains over a horizontal length of 630 m (resolution, 2 m). The second step was the generation of a succession of spheres along the slope profile to integrate a local roughness (Fig. 6). In the third step, the profile was extruded over 200 m along y-axis. To prevent a perfect alignment of the spheres along the slope, each row of spheres placed at the same height was offset by a random value between 0 and $2 \times R_{soil}$ (Fig. 7).

2.2.2 Forests

We compared the protective effect against rockfall of eight forests. Six forests were located close to the city of Grenoble, two forests were located near the village of Auzat in the French Pyrenees. The main species composing these forests were *Fagus* sylvatica, *Acer* Opalus, *Quercus* Pubescens, *Fraxinus* Excelsior. All forests were located on regular slopes from 20° to 35° in an active rockfall zone where no trace of forest management could be found. Eight field inventories using rectangular plots measuring 50×50 m were completed in each forest. The position of each inventory plot was selected randomly in the most homogeneous part of the forest. For each plot, the coordinates, the species and the diameter at breast height (measured 1.3 m from the

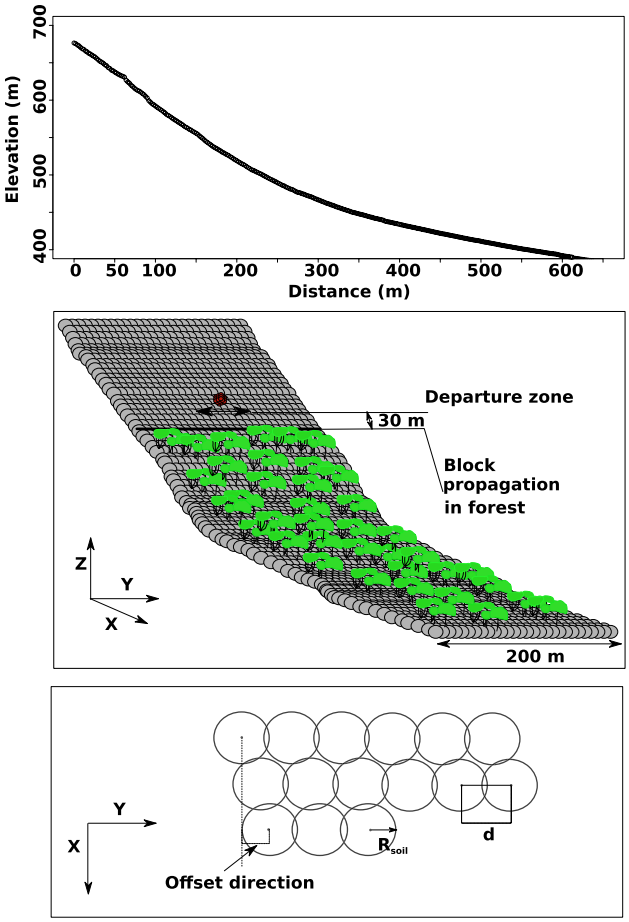

Fig. 7 Virtual slope used for simulations

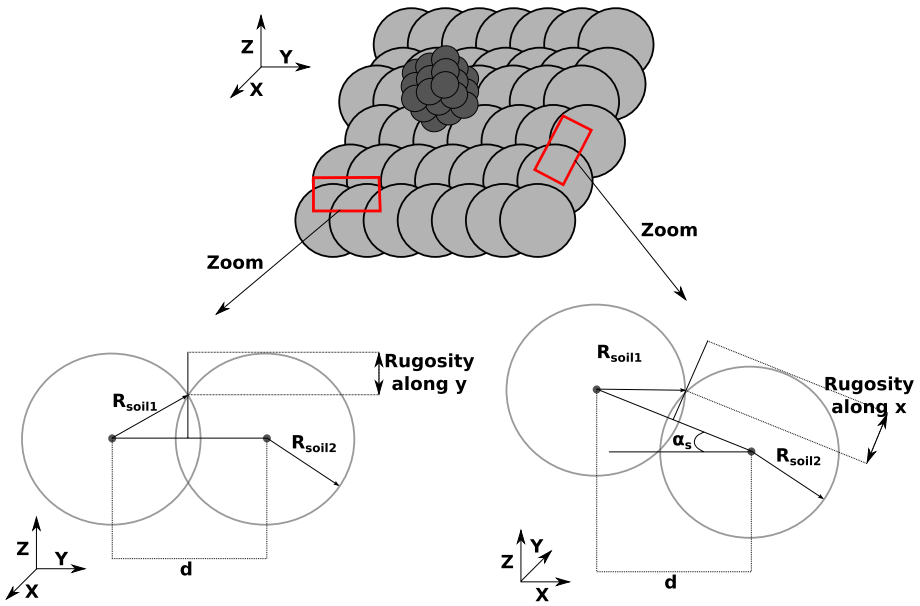

Fig. 6 Calculation of the roughness along the two X and Y axes. d is the distance between two spheres, R_{soil1} and R_{soil2} are the radii of two spheres and α_s is the local slope between the two spheres

ground at the upslope side of the stem) of each living stem with diameter ≥ 5 cm were recorded. In addition, we differentiated between stems belonging to the same coppice stool and individual trees. A coppice stool was defined as a stump with at least two stems of the same species. Absolute tree coordinates were measured using an ultrasound distance-measuring device (Vertex VL3, Haglöf, Sweden) and a compass on a tripod.

Most of the forests were composed of both coppice stools and single trees. The spatial stem distribution of each forest was analysed using the pair density function $g(r)$ (Ripley 1977; Stoyan 1987). The overall distribution of the stems in all plots had higher stem densities for distances $r \leq 1$ m (close to the trunk of the stools). This spatial stem aggregation is typical of coppice forests (Radtke et al. 2013). Following a similar analysis, we showed that the single trees were as randomly distributed as the centroid of the coppice stools.

For each forest inventoried, two virtual forests were generated covering the extent of the virtual slope: one integrates the spatial aggregation of the stems (A), the second is generated without spatial stem aggregation (NA).

The virtual aggregated forests were generated by first sampling the coordinates of the coppice stool centroids. Then, for each stool, the number of stems in the stool, the stool geometry and the diameter of each stem was sampled from the inventory data. When all the coppice stools were created, single trees were randomly generated until the total number of stems in the forest was reached. No stem superposition was allowed. The forests without spatial stem aggregation were generated by randomly sampling tree coordinates in a uniform distribution. The diameters associated with each stem were sampled from a distribution based on the field inventories.

To compare the stem aggregation between inventoried and virtual forests, the Clark and Evans aggregation index was computed with edge correction (Donnely 1978).

$$R_{\text{Clark}} = \frac{d_{\text{obs}}}{E_{\text{d}}} \tag{24}$$

$$E_{\text{d}} = \frac{1}{2 \times \sqrt{\frac{N_{E_{\text{d}}}}{S}}} \tag{25}$$

where d_{obs} is the mean nearest neighbour distance in the pattern, E_{d} is the mean nearest neighbour distance expected for a Poisson point process of the same intensity, $N_{E_{\text{d}}}$ is the number of trees in the forest and S is the surface of the forest calculated on the horizontal plane.

2.3 Comparative Analysis

A comparison between the DEM model and a process-based rockfall trajectory model Rockyfor3D (RF3D) was performed in this study. The efficacy of the forests to mitigate rockfall hazard was evaluated using indices calculated from the ratio between run-out distances along the slope, calculated from simulations with and without forest.

2.3.1 RF3D

RF3D is a model that simulates block trajectories on forested or non-forested slopes (Dorren 2012). The block, modelled as a sphere, propagates along a slope modelled by a DTM in raster format. The block propagation is modelled by a succession of phases of free flights, impacts on the slope surface and impacts on trees. The rolling motion of the block is considered as a succession of rebounds and the sliding of the block over the slope surface is not taken into account.

The computation of the rebound on the soil is made in two independent steps. The first step allows one to calculate the block trajectory deviation according to its incoming trajectory and slope. The second step calculates the translational and rotational velocities of the block after an impact on the soil based on the incident block velocities, block shapes, soil roughness and soil types (Dorren 2012). Rockyfor3D roughness is defined as the representative obstacle height at the slope surface. This parameter plays an important role in the calculation of the tangential coefficient of restitution.

The trees were modelled by cylinders distributed along the slope defined by the X and Y coordinates and the diameter of each tree.

The impact against a tree is detected when the distance between the block's position and the tree is lower than the sum of the tree radius and block equivalent radius. For each impact, the block kinetic energy reduction is calculated based on the eccentricity of the impact, the impact angle, the impact height, the species of the tree and the tree diameter (Dorren and Berger 2006). The kinetic energy reduction is distributed to the different components of the block velocity according to their contribution to the incident velocity. The change in the block trajectory after the impact against a tree is calculated based on the impact eccentricity.

RF3D perfoms a probabilistic analysis and several parameters are random variables. In particular, the parameters used to calculate the rebound are random variables determined by distributions calibrated with back-analyses of rockfall events. Furthermore, the block trajectory change during each rebound is also calculated by random sampling in distributions calibrated with experimental data (Dorren and Berger 2006).

2.3.2 Simulation Parameters

Input parameters associated with the block and the soil for the two models were first calibrated in order to obtain similar run-out distances without forest. These parameters were also used in all rockfall simulations with forest.

The parameters of the DEM contact law were set for impacts on a scree (Thoeni et al. 2014) (Table 2). The soil roughness of the profile was set equal to 0.1 m. A single starting point was considered ($X = 100$ m and $Y = 100$ m). The initial fall height, the block volume and block density were set equal to 5 m, 0.5 m^3 and 2.7 t/m^3, respectively. Before each simulation, the block orientation was randomly drawn to introduce variability in the simulations (different orientations were considered ranging from 0° to 180° in x, y and z directions). Three thousand simulations were performed with the DEM model.

The RF3D input parameters were calibrated to obtain a distribution of the block stopping distances similar to block propagations observed from the DEM simulations. Three thousand simulations were performed. In these simulations, the fall height and the block properties were set at the same values as those used in the DEM model. The calibrated values of the input parameters associated with the soil for RF3D are presented in Table 1.

The protective effect against rockfall hazard of the eight forests was tested with the DEM model and RF3D. For each forest, only 100 simulations were performed with the DEM model due the long computation time and 60,000 simulations were performed with RF3D. A propagation non-forested area measuring 30 m was defined down-slope of the rockfall release area (Fig. 7), to enable the blocks to reach a representative propagation velocity (15 m/s) when entering the forested zone (Dorren et al. 2007). To explore a wide range of block propagation in the forested zone, the X coordinate of the release location was set at $X = 100$ m and the Y coordinate was randomly chosen between 80 and 120 m (Radtke et al. 2013).

Table 1 Input parameters used for RF3D simulations

Soil	
Roughness [m]	0.04
Soil type	4: Talus slope
Resolution [m]	2
Block	
Shape	Cubic
Volume [m^3]	0.5
Density	2.7
Tree	
Species	100% Broadleaf

Table 2 Input parameters for the DEM model simulations

Soil	
Roughness [m]	0.1
Kn	1×10^6
κ^{soil}	0.05
$\frac{\alpha}{\alpha_{cr}}$	0.54
φ^{soil} [°]	30
Block	
Shape	Cubic
Volume [m^3]	0.5
Density	2.7
$D1$ [m]	0.794
φ^{b_t} [°]	30
E_b [MPa]	80×10^3
Trees	
MOE [MPa]	8.7×10^3
E_{plast} [Mpa]	2.1×10^3
E_{Unld} [Mpa]	5.3×10^3
σ_{Elast} [Mpa]	3.7×10^1
σ_{Rupt} [MPa]	9.4×10^1
τ	5×10^{-4}
Density	1.2
φ^{t_t} [°]	0
E_r [MPa]	1.5×10^3
κ^{b_t}	0.3
κ^{t_t}	0.3
M_a [Nm/rad]	7.5×10^6
K_{root} [Nm]	200×10^3

In a previous study, Toe et al. (2017) highlighted that the mechanical properties of the tree involved in the DEM model, which are directly linked to the tree species, had no significant influence on the block trajectory changes due to the impact on a tree. Therefore, the mechanical characteristics of the single trees and coppice stools are set to average values defined for beech *F. sylvatica* (Table 2).

2.3.3 Protective Capacity of Forests

The quantification of the protective capacity of the forests with respect to rockfall is generally based on indices based on the runout distance of the blocks or their kinetic energy at a given distance from the departure zone (Volkwein et al. 2011; Radtke et al. 2013). These indices are then compared for forested and non-forested situations. In this study, the indices used to quantify the protective capacity of forests were based on run-out distances along the slope, given that the indices based on block energies are less sensitive to forest effects (Radtke et al. 2013; Dupire et al. 2016).

Two indices were calculated from the results of the DEM model and RF3D:

$$PF^{50}_{DEM} = 1 - \frac{Dist^{50}_{WF_{DEM}}}{Dist^{50}_{NF_{DEM}}} \quad (26)$$

$$PF^{50}_{RF3D} = 1 - \frac{Dist^{50}_{WF_{RF3D}}}{Dist^{50}_{NF_{RF3D}}} \quad (27)$$

PF^{50}_{DEM} and PF^{50}_{RF3D} are the protection index determined from the run-out distances of the DEM model and RF3D. $Dist^{50}_{WF_{DEM}}$ and $Dist^{50}_{WF_{RF3D}}$ are, respectively, the distances where 50% of the blocks were stopped in the simulations with forest from the DEM model and RF3D. $Dist^{50}_{NF_{DEM}}$, $Dist^{50}_{NF_{RF3D}}$ are those for the simulations without forest.

Table 3 Dendrometric parameters for inventoried and virtual forests

Name	$Mean_D$ (cm)	Std_D (cm)	N	G (m^2 ha^{-1})	R_{Clark}
GR1	16.98	8.20	1172	32.74	0.58
$GR1_A$	17.25	8.14		32.52	0.60
$GR1_{NA}$	17.11	8.10		32.99	1.00
MO1	13.32	6.52	1920	43.33	0.69
$MO1_A$	13.31	6.41		42.91	0.67
$MO1_{NA}$	13.31	6.43		43.00	1.00
MO2	9.65	4.40	2508	26.78	0.73
$MO2_A$	9.64	4.38		26.68	0.70
$MO2_{NA}$	9.64	4.35		26.62	1.01
SP1	12.35	8.05	1668	28.47	0.65
$SP1_A$	12.04	7.66		28.71	0.68
$SP1_{NA}$	12.08	7.65		28.81	1.00
SP2	14.45	6.21	1956	38.00	0.82
$SP2_A$	14.46	6.16		37.98	0.82
$SP2_{NA}$	14.38	6.13		37.57	1.00
SP3	12.40	5.06	2552	35.98	0.80
$SP3_A$	12.37	5.05		35.62	0.79
$SP3_{NA}$	12.28	5.02		35.32	1.00
PY1	21.71	11.77	916	43.87	0.75
$PY1_A$	21.50	11.48		42.79	0.69
$PY1_{NA}$	21.38	11.36		40.56	1.00
PY2	21.84	7.70	972	40.92	0.69
$PY2_A$	21.56	7.62		39.9	0.67
$PY2_{NA}$	21.72	7.70		40.56	1.00

$Mean_D$ and Std_D are the mean value and standard deviation of the tree diameters

N and G are, respectively, the number of stem per hectare and the basal area of a forest

3 Results

3.1 Forest Generation

The generated virtual coppice forest (*A* and *NA*) had mean diameters ($Mean_D$), standard deviation of the diameters (Std_D) and basal areas (G) close to the inventoried forests (difference less than 1%) (Table 3).

Since the number of stems per hectare (N) is an input parameter for the forest generation, N values were the same for generated and inventoried forests. Differences between R_{Clark} values for virtual and inventoried forests varied from 2 to 5% (mean of the difference: 1.4%). A greater difference (8%) was observed for the PY1 forest. The absence of spatial aggregation for *NA* forests was confirmed by R_{Clark} values equal to 1.

3.2 Simulations Without Forest

The run-out distances along the slope from DEM model simulations were distributed over a small distance interval (the majority of the deposit areas ranged between 325 m and 375 m). The lateral dispersion of the blocks was also reduced (about 40 m) and preferential block deposit areas were observed around 330 m from the departure zone (Fig. 8).

Rockfall simulations without forest using RF3D were set to have block stopping distances similar to the DEM model simulations. Stopping distances from RF3D simulations are distributed over a larger distance interval compared to the DEM model (from 250 to 450 m). Moreover, the lateral dispersion of the blocks was twice as large in RF3D simulations (over 80 m at 350 m from the departure zone). For both models, the blocks were doing short bounces with low bounce heights ≤ 1 m and a propagation velocity ranging from 10 to 15 m/s.

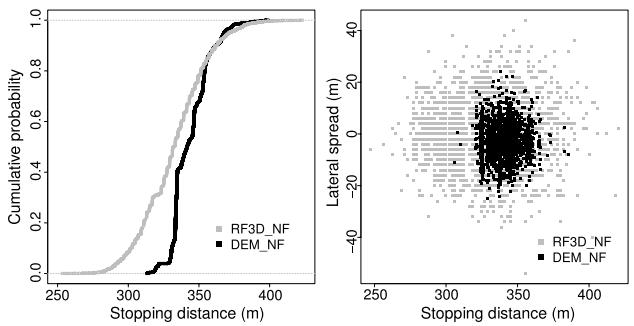

Fig. 8 Cumulative distribution of the run-out distance of the blocks and stopping positions of the blocks

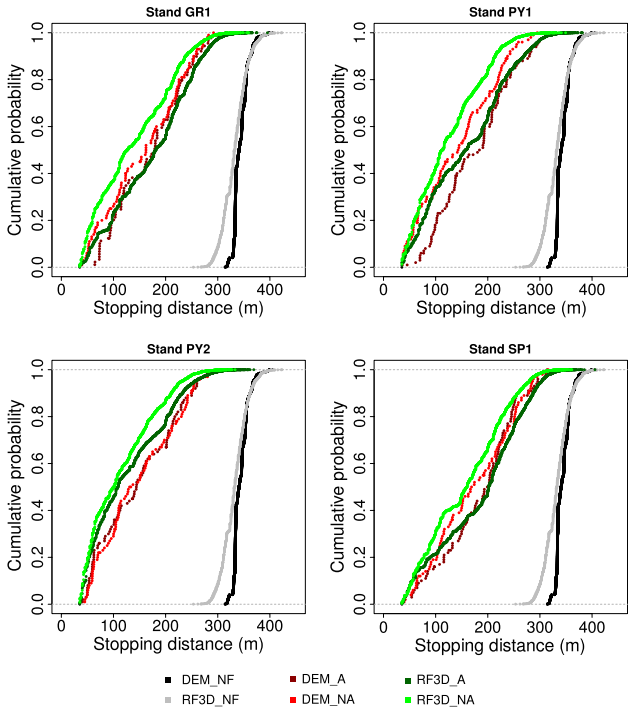

Fig. 9 Distribution of the block propagation distances for simulation with and without forest for the DEM model and RF3D

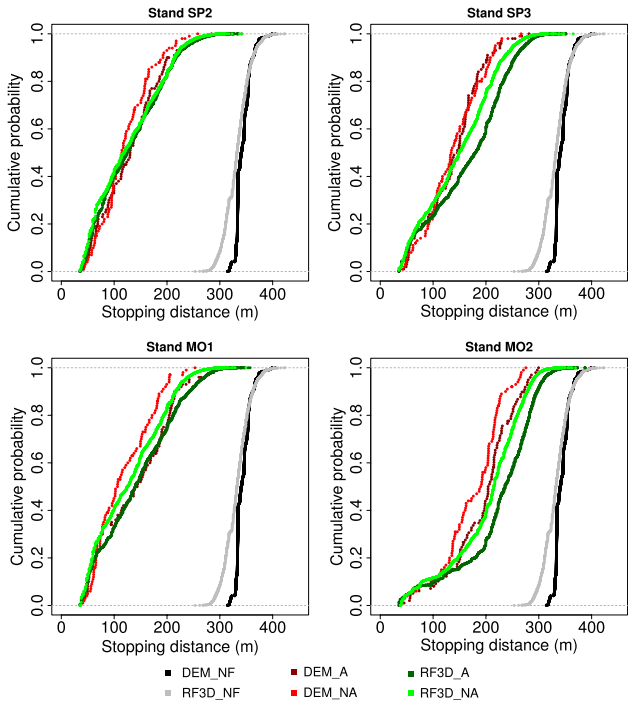

Fig. 10 Distribution of the block propagation distances for simulation with and without forest for the DEM model and RF3D

3.3 Simulations with Forest

Regardless of the model (DEM or RF3D), the run-out distances with forest (*A* and *NA*) were significantly smaller than those without forest (Figs. 9, 10). The distribution of the run-out distance distributions from the DEM model were close to those from RF3D.

In DEM simulations the run-out distances were slightly shorter for *NA* forests compared to *A* forests (Figs. 9, 10). The RF3D simulations also highlight that the run-out distances were shorter for *NA* forests compared to *A* forests (Figs. 9, 10).

The PF^{50}_{DEM} indices ranged from 0.4 to 0.6 and the PF^{50}_{RF3D} indices ranged from 0.3 to 0.6. The index values were lower for *A* forests compared to *NA* forests, which highlights that *A* forests have a smaller capacity to mitigate rockfall hazard for both models (RF3D and DEM) (Fig. 11).

The forest's capacity to mitigate rockfall hazard is ranked from 1 to 8, where 1 is associated with the least effective forest and 8 with the most effective forest (Fig. 11). The ranking of the forests slightly differs between *A* and *NA* forests. The SP1, MO2, GR1, SP3 forests usually receive the lowest scores while the SP2, MO1 and SP3 forests generally perform best.

PF^{50}_{DEM} indices tended to increase with increasing basal area and mean tree diameters (Fig. 12). A more pronounced trend was observed for PF^{50}_{RF3D} indices. No significant trend was observed between PF^{50}_{DEM} and the number of stems per hectare of forests. However, PF^{50}_{RF3D} tended to decrease with an increasing number of stems per hectare. The variation of PF indices as a function of the dendrometric parameters of the forests was not influenced by the spatial structure of forests regardless of the model used.

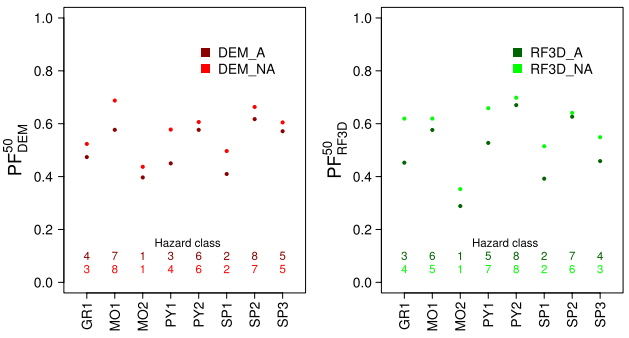

Fig. 11 PF^{50} indices of the different forests calculated from the DEM model and RF3D simulations. *DEM_A* and *DEM_NA* are the results from the DEM model for forests with spatial aggregation and forests without spatial aggregation. *RF3D_A* and *RF3D_NA* are the results from RF3D for forests with spatial aggregation and forests without spatial aggregation

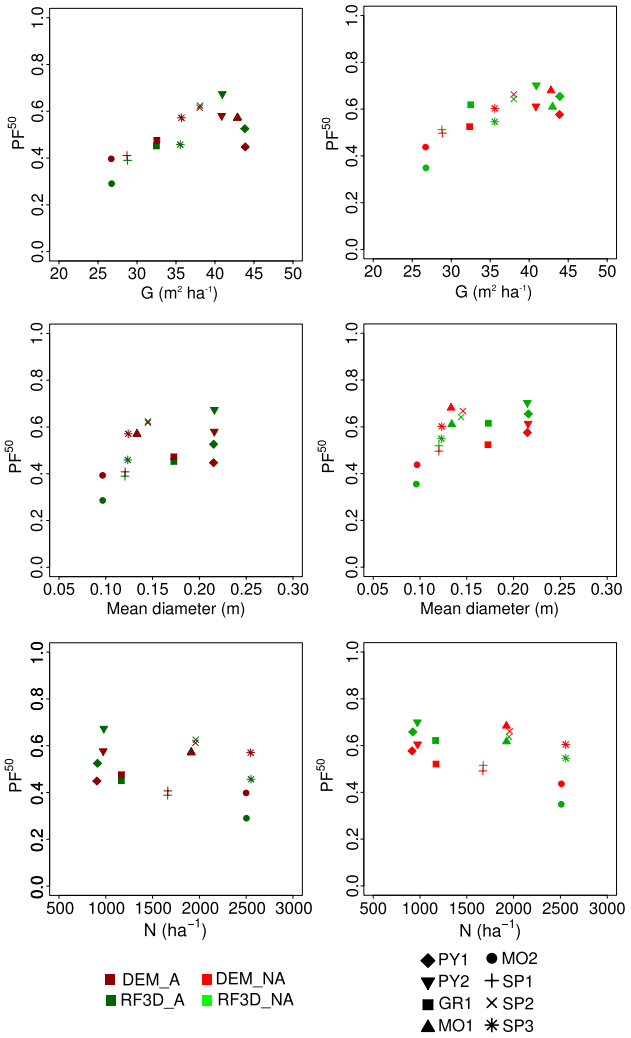

Fig. 12 PF^{50} indices as a function of the basal area (G), the mean diameter and the number of stems per hectare (N)

4 Discussion

4.1 Rockfall Propagation Without Forest

Rockfall simulations without forest are required to compare the results with simulations under forested conditions so as to assess the capacity of a forest to mitigate rockfall hazard. The input parameters of RF3D were calibrated by matching model run-out distances without forest to those obtained with the DEM model. No field data were available to calibrate or validate RF3D simulations. However, the energy lines obtained in the simulations varied between 32° and 25°. These values can be considered realistic (Jaboyedoff and Labiouse 2011).

Despite this correspondence between the two models, in RF3D the blocks are deposited over a long distance, 275 m to roughly 450 m measured from the departure zone, whereas in the DEM simulations most of the blocks stopped before 310 m. Moreover, RF3D simulations showed a lateral block dispersion that was twice as large as those with DEM. The higher variability of the propagation distances and lateral dispersion of the blocks in RF3D could be related to the high number of random variables used in RF3D and to the greater variation ranges of these variables compared to the DEM model. Indeed, the only source of variability in the DEM model was the initial orientation of the block. On the contrary, in RF3D, the sources of variability are the normal restitution coefficient and the block lateral dispersion after rebound on the soil and on the trees.

Several preferential block deposit areas, aligned along an axis perpendicular to the propagation direction of the blocks (Fig. 8) were observed in simulations performed using the DEM model. These preferential deposit areas were not observed in RF3D simulations where the block deposit was homogeneously distributed along the slope. This difference between the two models is likely related to a different modelling approach of the slope surface in the two models. In the DEM model, the soil is modelled by spheres that explicitly take into account soil roughness. The presence of a preferential deposit area in the vicinity of topographic breaks could be explained by the combined effect of the topography and the roughness, which leads to the creation of barriers. In RF3D, the soil is modelled by facets oriented using two angles: the slope and the facet orientation. However, soil roughness is implicitly taken into account in the calculation of the block rebound. The method used to model the soil leads to a smoothing of the topography and a better distribution of the stopping distances (Lambert et al. 2013).

4.2 Block Propagation Along a Forested Slope

Regardless of the model used for the simulations, all the forests tested showed a significant capacity to mitigate rockfall hazard. Similar run-out distances were observed for different forests using both models, in particular for the PY2, MO1 and MO2 forests (Figs. 9, 10). The DEM models and RF3D have almost the same capacity to model the protective effect of these forests.

Previous work based on the study of block propagations in coppice forests (Radtke et al. 2013), concluded that if the spatial structure of the forests is not taken into account in the simulation, an overestimation of the protective capacity of the forest against rockfall hazard can be expected. This result is confirmed in this study. In the DEM rockfall simulations, the *NA* forests have a higher capacity to mitigate rockfall hazard compared to *A* forests. However, this conclusion has to be considered with caution due to the small differences between the cumulative distributions of the block stopping distances for *A* and *NA* forests (e.g. SP3, SP2, PY2, GR1) and the lower number of simulations.

The ability of coppice forests to mitigate rockfall hazard was quantified using indices based on block stopping distances. The forests studied can significantly reduce run-out distances of the blocks and the classification of forests based on their efficacy is similar for both models used.

The ability of coppice forests to mitigate rockfall hazard slightly differs for the different forests. Their ability to mitigate rockfall hazard depends on their spatial structure (*NA* forests are more effective at stopping blocks compared to *A* forests) and their dendrometric characteristics. The influence of the dendrometric parameters on the forest's effectiveness in mitigating rockfall hazard slightly differs depending on the model used. In the DEM model, *G* has a significant influence on PF indices. In RF3D, PF indices are significantly influenced by *G*, *N* and the mean diameter. The significant influence of *G* on PF indices are in agreement with syvicultural guides that establish empirical relationships to characterize the protection capacity of forest based on the basal area (Gauquelin and Courbau 2006; Berger and Dorren 2007).

In this study, each PF index is calculated from simulations based on only one generation of a *A* or NA coppice forest. However, the coppice forest generation for an identical set of input parameters could lead to the creation of virtual forests with more or fewer spatial aggregations compared to the inventoried forests. These differences are due to multiple random processes involved in the virtual forest generation. The ranking of the different forests could therefore change if new virtual forests are generated.

A better characterization of the protective function of coppice forests could be achieved by generating more virtual forests for each inventoried forest. Then, for each virtual forest, a high number of rockfall simulations would have to be carried out to take into account the variability of blocks propagating along the slope. However, such a study would be too time-consuming when using the DEM model, since the computation time required for 100 single block propagations on a slope with forest is 72 h compared to 0.5 s for 100 simulations with RF3D (on the same computer).

For either rockfall model used (DEM or RF3D) and for identical dendrometric input parameters, a forest only composed of single trees mitigates rockfall hazard more effectively compared to a forest composed of single trees and coppice stools. Due to their spatial structure, coppice forests have small areas with a high stem density, but also larger areas with very low stem density. In the latter, blocks can accelerate, which eventually could lead to decrease the ability of the forest to mitigate rockfall hazard.

Silvicultural guides for the management of rockfall protection forests have been developed on the basis of empirical data that do not take the spatial structure of the forests into account (Gauquelin and Courbau 2006; Jean et al. 2012). In this paper, small differences were found between the protective function of *A* and *NA* forests. Therefore, it seems that the recommendations given in the silvicultural guides remain valid for both *NA* and *A* forests. However, in the case of coppice forests, a safety factor has to be considered when estimating the residual hazard below a coppice forest to avoid overestimating its protective function.

5 Conclusions and Perspectives

A new approach to model the propagation of blocks in forests was presented in this paper. Each of the forests studied significantly reduces the rockfall hazard for the block size considered. The results highlight that, even if the spatial forest structure has a small influence on the block propagation, it has to be taken into account in simulations to avoid overestimating the protective role of forests against rockfall hazards. In addition, we found that the basal area of the forest is the key indicator for the protective capacity against rockfall hazards compared to the other forest parameters considered.

One advantage of the DEM model, compared to classical rockfall models, is that it can explicitly model soil roughness, the block/soil, block/tree contacts and the shape of the block. Although the slope surface is modelled in detail in the DEM model, it remains an approximation of the real slope, and the deterministic approach of the DEM model cannot reproduce local slope variability. In RF3D, this problem can be partly taken into account using a probabilistic calculation of the rebound. Finally, DEM simulations are highly time-consuming compared to probabilistic lumped-mass rockfall models.

Further research has to be conducted in order to improve the DEM model. The next step in the DEM model development would be improving the modelling of the slope. This would allow taking into account the effect of the topography (e.g. corridors), which has a large influence on the rockfall propagation, into account. In addition, the influence of the surface roughness on the run-out of the blocks needs to be investigated to determine how accurately this parameter must be recorded in the field.

The block/soil contact is currently modelled with a contact law which needs to be calibrated and validated using real-scale impact experiments. These experiments would first validate the relevance of the contact law used to predict the run-out distance of the blocks and second to characterize different soil parameters for the slope surface and subsurface types commonly occurring in mountain areas.

Acknowledgements This research was funded by ANR SAMCO and ANR ALIEN-project. Irstea is part of Labex OSUG@2020 (ANR10 LABX56).

References

Andrew R, Hume H, Bartingale R, Rock A, Zhang R (2012) User's manual: Colorado rockfall simulation program. Technical report no. FHWA-CFL/-12-007, Central Federal Lands Highway Division, Federal Highway Administration

Bartelink H (1997) Allometric relationships for biomass and leaf area of beech (*Fagus sylvatica* L.). Annales des Sciences Forestires 54(1):39–50, doi:10.1051/forest:19970104

Berger F, Dorren L (2007) Principles of the tool Rockfor.net for quantifying the rockfall hazard below a protection forest. Schweizerische Zeitschrift fur Forstwesen 158(6):157–165, doi:10.3188/szf.2007.0157

Bertrand D, Bourrier F, Olmedo I, Brun M, Berger F, Limam A (2013) Experimental and numerical dynamic analysis of a live tree stem impacted by a Charpy pendulum. Int J Solids Struct 50(10):1689–1698. doi:10.1016/j.ijsolstr.2013.01.037

Bourrier F, Kneib F, Chareyre B, Fourcaud T (2013) Discrete modeling of granular soils reinforcement by plant roots. Ecol Eng 61(Part C):646–657. doi:10.1016/j.ecoleng.2013.05.002

Chopra AK (2011) Dynamics of structures, 4th edn. Prentice Hall, Upper Saddle River

Cundall PA, Strack ODL (1979) A discrete numerical model for granular assemblies. Gotechnique 29(1):47–65. doi:10.1680/geot.1979.29.1.47

Donnely K (1978) Simulations to determine the variance and edge effect of total nearest-neighbor distance. Cambridge University Press, Cambridge, pp 91–95

Dorren L (2012) Rockyfor3d (v4.1) revealed_transparent description of the complete 3D rockfall model. Technical report, ecorisQ

Dorren L, Berger F (2006) Stem breakage of trees and energy dissipation during rockfall impacts. Tree Physiol 26(1):63–71

Dorren L, Berger F, Jonsson M, Krautblatter M, Mölk M, Stoffel M, Wehrli A (2007) State of the art in rockfall forest interactions. Schweizerische Zeitschrift fur Forstwesen 158(6):128–141. doi:10.3188/szf.2007.0128

Dupire S, Bourrier F, Monnet JM, Bigot S, Borgniet L, Berger F, Curt T (2016) Novel quantitative indicators to characterize the protective effect of mountain forests against rockfall. Ecol Indic 67:98–107. doi:10.1016/j.ecolind.2016.02.023

Dupuy L, Fourcaud T, Stokes A (2005) A numerical investigation into factors affecting the anchorage of roots in tension. Eur J Soil Sci 56(3):319–327. doi:10.1111/j.1365-2389.2004.00666.x

Gauquelin X, Courbaud B (2006) Guide des sylvicultures de montagne - Alpes du Nord françaises, coédition cemagref - onf edn

Jaboyedoff M, Labiouse V (2011) Technical note: preliminary estimation of rockfall runout zones. NHESS 11:819–828. doi:10.5194/nhess-11-819-2011

Jancke O (2012) Quantifying the mechanical resistance of coppice trees against rockfall. PhD thesis, Hamburg

Jancke O, Dorren LKA, Berger F, Fuhr M, Kohl M (2009) Implications of coppice stand characteristics on the rockfall protection function. For Ecol Manag 259(1):124–131. doi:10.1016/j.foreco.2009.10.003

Jean L, Rey F, Dreyfus P (2012) Guide des sylvicultures de montagne pour les Alpes du Sud françaises. ONF, Irstea

Jonsson MJ, Volkwein A, Ammann WJ (2007) Quantification of energy absorption capacity of trees against rockfall using finite element analysis. Taylor & Francis Ltd, London

Lambert S, Bourrier F, Toe D (2013) Improving three-dimensional rockfall trajectory simulation codes for assessing the efficiency of protective embankments. Intl J Rock Mech Min Sci 60:26–36. doi:10.1016/j.ijrmms.2012.12.029

Lundström T (2009) Mechanical stability and growth performance of trees. PhD thesis, Universit de Fribourg

Olmedo I (2015) Étude expérimentale et numérique de l'efficacité d'ouvrage ligneux de génie biologique parre-pierres. PhD thesis, Institut National Des Sciences Appliquées, IRSTEA Grenoble

Olmedo I, Bourrier F, Bertrand D, Berger F, Limam A (2016) Discrete element model of the dynamic response of fresh wood stems to impact. Eng Struct 120:13–22. doi:10.1016/j.engstruct.2016.03.025

Plassiard JP, Donzé FV (2010) Optimizing the design of rockfall embankments with a discrete element method. Eng Struct 32(11):3817–3826. doi:10.1016/j.engstruct.2010.08.025

Quetel C (2005) Approche multi-échelle du comportement mécanique d'un arbre soumis l'impact d'un bloc rocheux. PhD thesis, Ecole Centrale de Lyon

Radtke A, Toe D, Berger F, Zerbe S, Bourrier F (2013) Managing coppice forests for rockfall protection: lessons from modeling. Ann For Sci 71:1–10. doi:10.1007/s13595-013-0339-z

Ripley BD (1977) Modelling Spatial Patterns. J R Stat Soc 39(2):172–212

Šmilauer V, Catalano E, Chareyre B, Dorofeenko S, Duriez J, Gladky A, Kozicki J, Modenese C, Scholts L, Sibille L, Stránský J, Thoeni K (2014) The Yade project. http://yade-dem.org/doc/

Stoyan D (1987) Statistical-analysis of spatial point-processes—a soft-core model and cross-correlations of marks. Biom J 29(8):971–980. doi:10.1002/bimj.4710290811

Thoeni K, Lambert C, Giacomini A, Sloan SW (2013) Discrete modelling of hexagonal wire meshes with a stochastically distorted contact model. Comput Geotech 49:158–169. doi:10.1016/j.compgeo.2012.10.014

Thoeni K, Giacomini A, Lambert C, Sloan SW, Carter JP (2014) A 3d discrete element modelling approach for rockfall analysis with drapery systems. Int J Rock Mech Min Sci 68:107–119. doi:10.1016/j.ijrmms.2014.02.008

Toe D, Bourrier F, Olmedo I, Monnet JM, Berger F (2017) Analysis of the effect of trees on block propagation using a DEM model: implications for Rockfall modelling. Landslides. pp 1–12, doi:10.1007/s10346-017-0799-6

Volkwein A, Schellenberg K, Labiouse V, Agliardi F, Berger F, Bourrier F, Dorren L, Gerber W, Jaboyedoff M (2011) Rockfall characterisation and structural protection–a review. Nat Hazards Earth Syst Sci 11:2617–2651. doi:10.5194/nhess-11-2617-2011

Xinpo L, Siming H, Yu L, Yong W (2010) Discrete element modeling of debris avalanche impact on retaining walls. J Mt Sci 7(3):276–281. doi:10.1007/s11629-010-2019-x